Measurement of the Lamb shift in the $n=4$ state of $^4He^+$

J. J. Bollinger,* S. R. Lundeen, and F. M. Pipkin
Lyman Laboratory of Physics, Harvard University, Cambridge, Massachusetts 02138
(Received 30 June 1983; revised manuscript received 18 July 1984)

The separated oscillatory field technique was used with a 120-keV $^4He^+$ beam to make a zero-magnetic-field measurement of the $n=4$ Lamb-shift interval in $^4He^+$. Excited $^4He^+$ ions were created by collisions in a cell filled with N_2 gas. The $4\,^2S_{1/2}$ state population was monitored by observing its decay to the $2\,^2P$ state with a large solid-angle NO photoionization detector. The $n=4$ to 2 light (121.5 nm) decreased when the microwave field induced transitions from the $4\,^2S_{1/2}$ to the $4\,^2P_{1/2}$ state. The value obtained for the Lamb shift was 1769.16 ± 0.84 MHz. This result agrees satisfactorily with previous measurements and with the theoretical value for this interval. The experimental uncertainty is dominated by systematic effects attributed to the presence of overlapping cascade signals.

I. INTRODUCTION

Measurements of the Lamb shift of hydrogenic ions provide sensitive low-energy tests of quantum electrodynamics (QED). The most precise Lamb-shift measurements to date have been made in hydrogen[1–4] where the sub-10-ppm experimental precision is comparable to the 4 ppm uncertainty in the theoretical value due to the error in the experimental value for the proton radius used to calculate the correction due to the finite nuclear size.[5–7] Improvements in the measurement of the proton charge radius are required to reduce the uncertainty in the finite nuclear size contribution and to improve substantially the sensitivity of measurements of the hydrogen Lamb shift as tests of QED.

Even though substantial improvements in the measurements of the proton charge radius are not expected in the near future, the charge radius of the $^4He^+$ nucleus has been determined more than an order of magnitude more precisely than the charge radius of the proton. From measurements of the $2\,^2S_{1/2}$-$2\,^2P_{3/2}$ interval in muonic helium, the charge radius of the α particle has been determined to be 1.673(1) fm.[8,9] This agrees with the less precise, but direct, electron scattering measurement of 1.674(12) fm.[10] Because of the precise determination of the $^4He^+$ nuclear charge radius, the finite nuclear size contribution to the uncertainty in $^4He^+$ Lamb-shift calculation is negligible. $^4He^+$ Lamb-shift measurements potentially provide, therefore, especially sensitive tests of the QED calculations.

The most precise calculations of Lamb-shift intervals with different Z (nuclear charge) have been made by Erickson[5] and Mohr.[6] The two calculations differ in their estimates of the higher-order binding corrections to the self energy of the electron. Recently Sapirstein[7] has reported a calculation of the electron higher-order self-energy corrections for the $1s$ state of hydrogen which is reasonably consistent with Mohr's result for hydrogen. While the Lamb-shift interval scales approximately as Z^4, the Erickson-Mohr difference scales approximately as Z^6. High-Z measurements in general, and helium compared to hydrogen in particular, therefore offer an enhanced sensitivity for determining the correctness of these calculations.

Figure 1 compares hydrogen and helium Lamb shifts in the categories discussed above and in the experimental precision of the measurements. The best $^4He^+$ Lamb-shift measurements[11–14] to date are a factor of 10 less precise than the hydrogen measurements and are unable to take advantage of their sensitivity for testing QED. The possibilities offered by helium for sensitively testing QED and the need for a He^+ Lamb-shift measurement with greater experimental precision have motivated the Lamb-shift measurement in helium using the fast beam, separat-

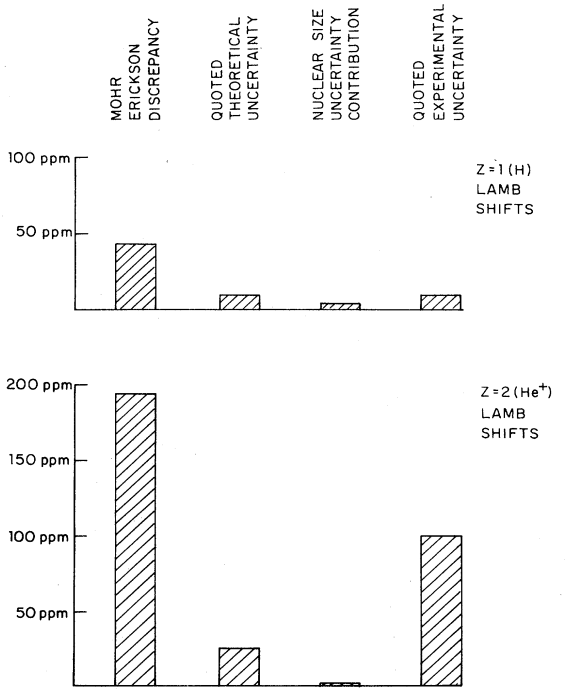

FIG. 1. Comparison of helium and hydrogen Lamb shifts.

ed oscillatory field technique which is the subject of this paper. This technique was used previously in this laboratory to make precise fine-structure measurements in hydrogen.[1,15–17] The $n=4$ $^2S_{1/2}$-$^2P_{1/2}$ Lamb shift was chosen as an experimentally convenient Lamb-shift interval to measure using this technique.

Table I lists the most precise experimental determinations[18–20] and theoretical calculations[5,6] of the $n=4$ $^2S_{1/2}$-$^2P_{1/2}$ Lamb shift in $^4He^+$. The theoretical values have been updated by using the precise muonic helium determination of the $^4He^+$ nuclear charge radius.[9] Mohr has only evaluated Lamb-shift intervals for $n=1,2$. An estimate of what Mohr's value for the $n=4$ He^+ Lamb-shift interval would be has been obtained by multiplying Mohr's $n=2$ He^+ Lamb shift by the ratio of Erickson's $n=4$ and $n=2$ He^+ Lamb shifts. This assumes that the ratio of the Erickson-Mohr difference, divided by the Lamb shift, does not change with n. This ratio does, in fact, increase slightly from $n=1$ to $n=2$ in hydrogen.[21] The more precise indirect determinations were obtained by subtracting the measured $n=4$ $^2S_{1/2}$-$^2P_{3/2}$ interval from the total fine-structure interval $\nu(4\,^2P_{3/2}$-$4\,^2P_{1/2})$ $=21\,949.124(41)$ MHz.[5] All the experimental determinations listed in Table I agree with the theoretical calculations. For a complete list of the many other, less precise $n=4$ He^+ Lamb-shift measurements, see Ref. 22.

The precision of the experimental $n=4$ He^+ Lamb shifts is disappointingly behind that of the theoretical calculations. The best direct experimental determination is only a 1130-ppm measurement. A major systematic problem common to most of the $n=4$ He^+ measurements has been contributions to the Lamb-shift resonance signal due to overlapping transitions in higher-n states. A technique to identify and account for cascade contributions was developed in this experiment and is described in Sec. II along with the rest of the experimental method and apparatus. Section III discusses the data collection procedure. Section IV gives the analysis of the data along with a discussion of the systematic corrections to the experimental line center. Section V compares the result of this measurement with the previous measurements and theoretical calculations.

II. EXPERIMENTAL METHOD AND APPARATUS

Figure 2 shows the energy-level diagram for the $n=4$ manifold of $^4He^+$ together with the lifetimes of the different levels. The short, 0.78-nsec lifetime of the $4\,^2P_{1/2}$ states produces a natural linewidth for the $4\,^2S_{1/2}$-$4\,^2P_{1/2}$ transition of 200 MHz and a line Q of less than 10. In this experiment, a fast atomic beam and two separated microwave spectroscopy regions[1,15,23] were used to obtain subnatural linewidths for this transition.

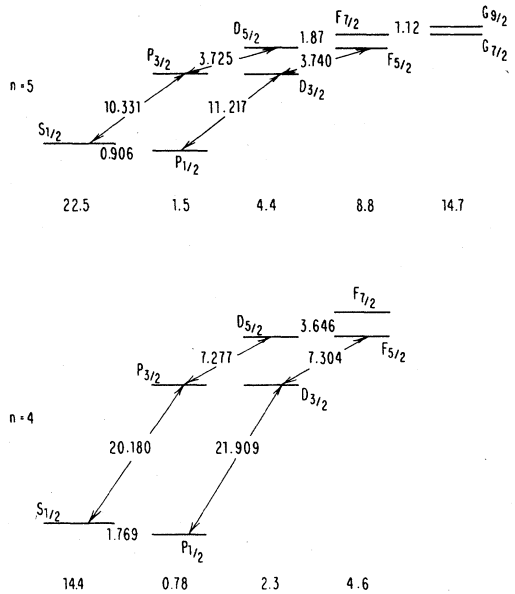

FIG. 2. Energy splittings (MHz) and lifetimes (ns) in the $n=4,5$ manifolds of $^4He^+$.

Figure 3 gives a sketch of the experimental layout. A magnetically analyzed beam of 120-keV He^+ ions from a small, commercially built accelerator was directed through a short, 4-cm-long cell filled with nitrogen gas at 10—40 mTorr pressure. Excited He^+ ions were created in collisions of the fast He^+ beam with N_2 gas molecules. The $4\,^2P$ He^+ ions decayed almost immediately after being created and traveled on the average less than 2 mm down the beam line. After passing through a vacuum baffle isolating the excitation cell from the rest of the vacuum system, the He^+ ions passed through a K-band waveguide cavity and entered the separated oscillatory field (SOF) region. The SOF region consisted of identical, 0.7-cm-wide, rectangular 50-Ω coaxial transmission lines separated by a small distance (typically 0.00, 0.32, or 0.64 cm). After the SOF spectroscopy region, the $4\,^2S_{1/2}$ level

TABLE I. Most precise experimental and theoretical determinations of the $n=4$ He^+ Lamb shift.

Experimental values (MHz)	Method	Reference	Theoretical values (MHz)	Reference
1769(2)	direct, bottle	18	1769.132(46)[b]	5
1768(5)	direct, bottle	19	1768.789(46)[b,c]	6
1768.5(0.8)[a]	indirect, bottle	20		
1769.4(1.2)[a]	indirect, bottle	18		

[a]The indirect values were obtained by subtracting the measured $4\,^2P_{3/2}$-$4\,^2S_{1/2}$ interval from $\nu(4\,^2P_{3/2}$-$4\,^2P_{1/2})=21\,949.124(41)$ MHz.

[b]Adjusted using 1.673(1) fm as the He^+ rms nuclear charge radius.

[c]Mohr's $n=4$ value was estimated by multiplying his $n=2$ Lamb shift by the ratio of Erickson's $n=4$ and $n=2$ values. Erickson's uncertainty was assigned to this value.

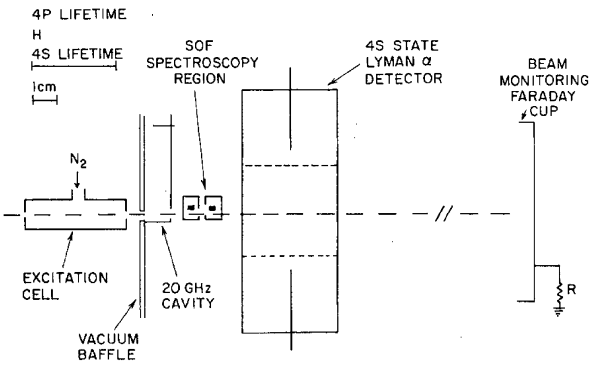

FIG. 3. The experimental layout.

population was monitored by observing its decay (121.5 nm) to the 2^2P state with a large solid angle vacuum ultraviolet photoionization detector.

By applying microwave power near the $n=4$ $^2S_{1/2}$-$^2P_{1/2}$ resonance frequency to the SOF region, some of the $4^2S_{1/2}$ state population was transferred to the short lived $4^2P_{1/2}$ state, resulting in a decrease in the $4^2S_{1/2}$ state population and in the output in the photodetector. The 0° and 180° quenching signals are defined to be the percent change in the output of the photodetector when the phase difference between the microwave field in the two SOF regions is 0° and 180°, respectively. Specifically,

$$S^0=(N^{\text{off}}-N^0)/N^{\text{off}}\,,$$
$$S^{180}=(N^{\text{off}}-N^{180})/N^{\text{off}}\,, \tag{1}$$

where N is the output of the photodetector normalized to the beam intensity as monitored by the Faraday cup at the end of the beam line. The average quench signal, $\bar{Q}$ is defined to be the average of S^0 and S^{180}; the interference signal, I, is defined to be the difference between S^0 and 180°

$$\bar{Q}=(S^0+S^{180})/2\,,$$
$$I=S^0-S^{180}\,. \tag{2}$$

The line profiles of the interference and average quench signal were observed in zero magnetic field by sweeping the frequency of the applied microwave field.

While the width of the average quench signal is determined by the natural linewidth and the transit time through one of the SOF regions, the width of the interference signal is determined by the transit time between the two SOF regions.[15,23] For transit times greater than the lifetime of the $4P$ state, the interference signal linewidth is smaller than the natural linewidth. In addition the interference signal size decreases exponentially with the separation between the SOF regions. If the determination of the resonance signal line center is limited by signal-to-noise ratio, very little is gained by separating the two SOF regions. The experiment, however, like many precision experiments, is not limited by signal-to-noise ratio, but by systematic effects. At the expense of some loss of signal-to-noise ratio, the interference signal minimizes many known systematic errors and provides experimental means for the investigation of other systematic effects. For instance, the interference signal line center is much less sensitive than the quench signal line center to a change in the microwave power as a function of frequency across the line. Reference 24 discusses the advantages of subnatural linewidth techniques in reducing systematic effects.

Because the $4^2S_{1/2}$ state is not metastable (14.4 nsec lifetime) and states with $n>4$ are excited in the excitation cell, the experiment was carried out in the presence of cascading light from states with $n>4$. Figure 2 shows that the $n=5$ $J=\frac{5}{2}\leftrightarrow\frac{7}{2}$ transitions at 1.87 GHz are only 100 MHz away from the $n=4$ Lamb-shift transition. Since the $5F$ state has a detectability of 0.27 in $n=4$ to 2 light and a lifetime of 8.8 ns, these transitions contribute significantly to the unquenched resonance signal. To isolate these and other possible overlapping transitions from the $n=4$ Lamb-shift resonance, an additional microwave region consisting of a waveguide cavity resonant at 20.180 GHz was used before the SOF region to quench the $4^2S_{1/2}$ states by driving the $4^2S_{1/2}\rightarrow 4^2P_{3/2}$ transition. This made possible the observation of any contributions due to overlapping transitions in higher n states which could then be subtracted from the Lamb-shift signal. With no quenching of the $4^2S_{1/2}$ states, let I_{nq}, $\bar{Q}_{\text{nq}}$, and $N_{\text{nq}}^{\text{off}}$, respectively, be the interference signal, average quench signal, and the beam normalized photodetector output with no microwave power applied to the SOF spectroscopy region. Similarly let I_q, $\bar{Q}_q$, and N_q^{off} be the same quantities with the $4^2S_{1/2}$ states quenched by the 20 GHz quenching cavity. The subtracted interference and quench signals are defined by

$$I_{\text{sub}}=I_{\text{nq}}-(N_q^{\text{off}}/N_{\text{nq}}^{\text{off}})I_q\,,$$
$$\bar{Q}_{\text{sub}}=\bar{Q}_{\text{nq}}-(N_q^{\text{off}}/N_{\text{nq}}^{\text{off}})\bar{Q}_q\,. \tag{3}$$

If the unquenched signals are the sum of the Lamb shift and cascade signals and the 20 GHz field does not affect the populations of those $n>4$ states which contribute to the cascade signals, then I_{sub} and $\bar{Q}_{\text{sub}}$ are free of cascade contributions.

Figure 4 gives an example of interference signal data taken with 0.32 cm separation between the SOF interaction regions. The contribution of $n>4$ overlapping transitions is approximately 8% of the $n=4$ Lamb-shift contribution and produces a 2 MHz upshift in the resonance line center of the unquenched Lamb-shift signal. The quenched interference signal is centered approximately at 1870 MHz. This is consistent with the $n=5$ $J=\frac{5}{2}\leftrightarrow\frac{7}{2}$ transitions being the major cascade contribution to the unquenched interference signal. Because of the large cascade contributions to the unquenched interference signal, the subtraction technique must work well to make a precision measurement of the Lamb shift.

Details of the experimental apparatus and its construction are given in Ref. 25. Since the experiment was done in zero magnetic field by varying the frequency applied to the SOF spectroscopy region, the SOF microwave system was a critical component of the experiment. Precision microwave components were used for all parts of the SOF

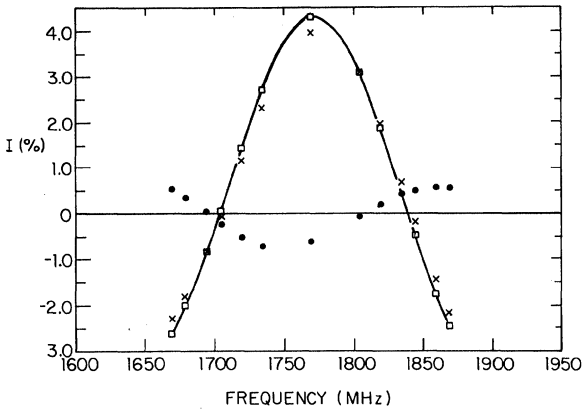

FIG. 4. Raw unquenched (×), quenched (●), and subtracted (□) interference data for a SOF separation of 0.32 cm and microwave power of 0.312 W per region. For these data $N_q^{\text{off}}/N_{\text{nq}}^{\text{off}}$ was 0.551. The line is drawn through the subtracted interference data.

microwave spectroscopy system. By carefully measuring the reflection coefficients and attenuation of the individual components, the relative power sampled by the ions in the center of the interaction region was determined to ±0.9% across the 300 MHz bandwidth used in the experiment.

The large solid angle Lyman-α (121.5-nm) detector consisted of six NO photoionization chambers with rectangular MgF_2 windows which totally surrounded the beam. Details of the construction and operation of the detector are given in Refs. 25 and 26. The detector was operated in the proportional mode with the external housing at negative voltage and the collection electrodes at ground. Typically the detector was operated with a gain of 10 to 50. The average fractional solid angle subtended by the photodetector over its 3.5 cm length was greater than 0.55. The combined detection efficiency resulting from the 2-mm MgF_2 window transmission and the NO photoionization quantum efficiency was estimated to be 35%. Consequently the overall detection efficiency for Lyman-α photons was approximately 20% over the 3.5 cm length of the detector. The high detection efficiency of the large solid-angle detector compensated for the rapid loss of $4s$ states due to the short $4s$ state lifetime and provided the signal-to-noise ratio necessary to make a precision measurement.

The cavity used to quench the $4s$ states was constructed from a shorted section of WR-42 waveguide. The cavity was resonant at 20.180 GHz with a Q of approximately 2000. Microwave power was supplied by a Raytheon 2K33 klystron electronically locked to the resonant frequency of the cavity.

Three oil diffusion pumps were used to produce a vacuum of better than 1.0×10^{-6} Torr in the beam line outside the excitation cell chamber. Liquid-nitrogen traps were used to minimize backstreaming of diffusion pump oil into the beam line. The beam line was constructed out of nonmagnetic materials to minimize unwanted magnetic fields. Three pairs of orthogonal Helmholtz coils were used to cancel the earth's magnetic field to less than 30 mG over the spectroscopy region.

III. DATA COLLECTION PROCEDURE

Because of the modulations and drifts in the beam intensity, data were taken by rapidly switching the SOF fields between the 0°, off, 180°, and off states. Each state of the microwave field was 48 msec long. A sequence of the four states listed above was a cycle. One point was 500 cycles long. The photodetector output, the Faraday-cup output, and the power monitoring diode voltage were fed into three voltage to frequency converters (VFC). The output pulses of the VFC's were fed into a system of synchronous counters. Each counter corresponded to a particular signal (photodetector output, beam current, or microwave power) and counted during a particular rf state. At the end of a point, a minicomputer read the counters and calculated the interference and quench signals according to Eqs. (1) and (2) with additional corrections for drifts in microwave power.[25] Three identical points were taken and the average and standard deviation of the average were calculated. At a given frequency, a set of three points without quenching of the $4^2S_{1/2}$ states was taken followed by a set of three points with quenching of the $4^2S_{1/2}$ states (or vice versa). The subtracted signals were then calculated from Eq. (3) using the group averages of the quenched and unquenched signals. The ratio $(N_q^{\text{off}}/N_{\text{nq}}^{\text{off}})$ of the beam normalized photodetector outputs with and without quenching of the $4^2S_{1/2}$ states varied by less than 0.5% over a period of several hours. Consequently errors in the subtracted signals due to drifts in $(N_q^{\text{off}}/N_{\text{nq}}^{\text{off}})$ over the 15 min of data taking time needed to obtain the two groups of quenched and unquenched data were negligible.

In general, data were taken at many frequencies in groups or runs characterized by the type of data and the experimental conditions during the time period of the run. Data used in the calculation of the interference signal raw centers were taken in frequency pairs of nominally equal interference signal height, typically centered about 1769 MHz. A symmetric point line center was calculated for each pair of frequencies as described in the next section. Figure 4 shows typical interference signal symmetric point data.

After a symmetric point data run was made, the direction of propagation of the microwave field was reversed in the SOF region. This canceled any first-order Doppler shift due to a slight deviation of the ion beam and SOF spectroscopy region from being perpendicular. After a Doppler-reversed pair of runs was obtained, the vacuum system was opened and the time order of the SOF interaction regions were reversed. Two Doppler reversed runs were taken with the reversed time order of the SOF interaction regions. The average of all four runs is free of first-order Doppler shifts and first-order phase errors between the two SOF transmission lines.

Data were taken with different microwave power levels of the SOF fields and with different separations of the SOF interaction regions. A variation of the SOF microwave power provided information on the total ac Stark

TABLE II. Summary of the configurations at which data were taken and the characteristics of the interference signals.

Separation (cm)	Power	I_{nq} size peak height (%)	Normalized I_q[a] peak height (%) at 1869	I_{sub} size peak height (%)	I_{sub} width (FWHM, MHz)
0.00	high	10.5	0.7	10.3	204
0.00	medium	4.8	1.1	4.6	193
0.00	low	1.4	0.4	1.4	189
0.32	high	4.0	0.3	4.4	135
0.32	medium	1.4	0.6	2.0	127
0.64	high	1.7	0.5	2.1	102
2.29	high	0.41	0.38	0.063	41.5
2.92	high	0.26	0.23	0.041	34.3

[a]The normalized I_q is given by $(N_q^{off}/N_{nq}^{off})I_q$.

shift. In addition, the $n>4$ overlapping transitions were saturated and contributed more significantly to the unquenched signal at low SOF microwave powers. Consequently, changing the SOF microwave power also provided a test of the subtraction technique. Changing the separation of the SOF interaction regions changed the width of the interference signal and permitted the investigation of a variety of systematic effects. Changing the separation also changed the relative sizes of the Lamb shift and overlapping transitions and therefore served as a test of the subtraction technique. If the separation is several times the mean distance which the $4\,^2P_{1/2}$ state survives, the $n=4$ Lamb-shift signal will be essentially zero and I_{nq} and I_q only differ by the normalization factor (N_q^{off}/N_{nq}^{off}). The presence of a nonzero interference signal in I_{sub} at wide separations would indicate a failure of the subtraction technique.

Table II gives a summary of the interference symmetric point data in this experiment. Data were taken at three narrow separations, 0.00, 0.32, 0.64 cm, and three different power levels. The high-, medium-, and low-power levels were in an approximate ratio of 12:4:1 with 1.03 W per interaction region as the power used for the high-power level. Wide separation data were taken at two separations but only at the high-power level.

IV. ANALYSIS OF THE DATA

The object of the data analysis is to extract from the measured line profile a value for the frequency of the $4\,^2S_{1/2}$-$4\,^2P_{1/2}$ Lamb-shift transition. One approach to doing this is to generate a theoretical simulation of the experimental line shape and fit the theoretical simulation to the experimental data with the Lamb-shift transition frequency as one of the free parameters. Theoretical simulations of the line shape were done and are described later. The complicated nature of the simulations and the lengthy computer time required to generate them precluded using the simulations as a fitting function for the data. The characteristics of the theoretical line shape were studied and an algorithm for determining the line center was developed.

Because there is no hyperfine structure, all electric dipole transitions in the $4\,^2S_{1/2}$-$4\,^2P_{1/2}$ manifold have the same frequency. If states outside the $4\,^2S_{1/2}$-$4\,^2P_{1/2}$ manifold are neglected and the rotating-wave approximation is used, it can be shown that for the SOF spectroscopy fields used in this experiment, the experimental line shape is symmetric about the $n=4$ Lamb-shift transition frequency.[25] The first-order effects of the counter rotating component and of states outside the $4\,^2S_{1/2}$-$4\,^2P_{1/2}$ manifold are small shifts in the line center. These shifts are, respectively, the Bloch-Siegert and ac Stark shifts. Computer simulations showed that any asymmetries introduced by higher-order effects can, for the purposes of this experiment, be neglected.

With the above symmetry property of the line shape, the following procedure can be used to determine the Lamb-shift transition frequency. For each pair of symmetric point frequencies F^+,F^- and signals $I(F^+),I(F^-)$, the symmetric point center F_c is defined by

$$F_c=\tfrac{1}{2}(F^++F^-)+\frac{I(F^+)-I(F^-)}{I'(F^-)-I'(F^+)}\,, \tag{4}$$

where $I'(F)$ is the derivative of the interference signal I with respect to the frequency F. If the interference signal is asymmetric, F_c will depend on the choice of the symmetric point frequencies. The symmetric points method provides, therefore, an efficient means of determining both the symmetry and the line center of the interference signal. If the interference signal is symmetric, the Lamb-shift transition frequency can be determined by correcting the symmetric points line center for the Bloch-Siegert and ac Stark shifts and any other known systematic shifts.

Due to imperfections in the microwave system, the microwave power varied over the line profile and through the dependence of the signals on the power introduced an apparent asymmetry. Before the symmetric point method could be used it was necessary to correct the signals to what they would be for a constant microwave field at the beam. Two methods were employed to determine the variation of the microwave power across the line profile. As mentioned previously standard microwave measurement techniques were used to determine the relative microwave power to $\pm 0.9\%$ over a 300 MHz bandwidth centered at 1769 MHz. The average quench signal, $\bar{Q}_{sub}$, was used as an independent check of this calibration. The average quench signal was very broad, [full width at half

maximum (FWHM) =600 MHz] and had no structure over the region used to measure the interference signal.

The power dependence of the average quench signal was modeled with a power law

$$\bar{Q}_{\text{sub}} \propto P^{\beta}, \tag{5}$$

where P is the average power in the two interaction regions and β is a slowly varying function of frequency and power. β was measured experimentally for all the frequencies in each narrow separation configuration. Values for β determined from the simulations agreed with the experimentally determined values to better than 3%. To first order the relative power difference $[(P^+-P^-)/P_0]$, where $P^+=P(F^+)$, $P^-=P(F^-)$, and P_0 is the nominal power for the experimental configuration, is given by

$$\frac{P^+-P^-}{P_0}=\frac{1}{\beta}\frac{\bar{Q}_{\text{sub}}(F^+)-\bar{Q}_{\text{sub}}(F^-)}{[\bar{Q}_{\text{sub}}(F^+)+\bar{Q}_{\text{sub}}(F^-)]/2}. \tag{6}$$

The relative power asymmetry was calculated from Eq. (6) for all the narrow separation configurations and averaged. The result is given in Fig. 5 along with the microwave derived power asymmetry. The two calibrations differ. By adding a 1% per 100 MHz sloping background to the microwave measurement derived calibration, the two power asymmetries can be made to agree.

This discrepancy between the two calibrations was not resolved. By defining and measuring a local power law for the interference signal similar to Eq. (5), power asymmetry corrections for the interference signal can be calculated for both power calibrations. This was done for all the narrow separation configurations. Within the uncertainties of the calculation, the quench signal derived power calibration removes the raw interference signal asymmetries in all 6 narrow separation configurations. The microwave measurement derived power calibration does not. The removal of the interference signal asymmetries in all 6 narrow separations is compelling evidence for the correctness of the quench signal derived power calibration. Consequently it was assumed to be the correct power calibration. Table III gives the raw symmetric points centers for the 0.00 cm, high-power configuration calculated using the quench signal derived power corrections. The average of the symmetric power corrected centers for each narrow separation configuration is given in Table IV.

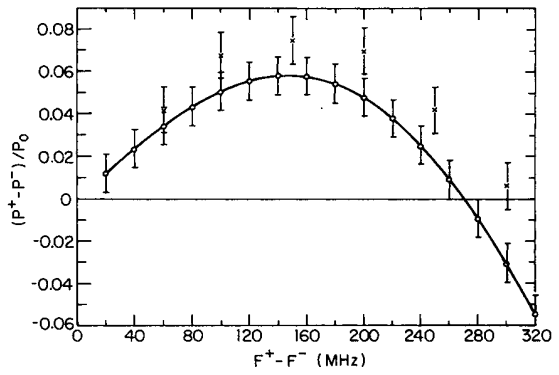

FIG. 5. Comparison of the microwave measurement (□) and the quench signal (×) derived power asymmetries.

TABLE III. The raw and corrected symmetric point centers for the 0.00 cm, high-power configuration.

F^-, F^+ (MHz)	Raw[a] centers (MHz)	Power correction (MHz)	Corrected center (MHz)
1719, 1819	71.462(60)	−0.995(163)	70.467(174)
1694, 1844	71.365(53)	−0.604(93)	70.761(107)
1674, 1864	71.029(57)	−0.344(59)	70.685(82)
1669, 1869	70.906(53)	−0.282(51)	70.624(74)
1644, 1894	70.648(67)	−0.006(20)	70.624(70)

[a]The raw centers are the averages of two complete sets of four runs.

Computer simulations of the experimental line shape were used to calculate the Bloch-Siegert and ac Stark shifts. The electric field inside the SOF rectangular coaxial transmission lines was calculated by solving Laplace's equation on a 240×240 grid by a relaxation method. Due to the small size of the rectangular transmission line, the electric field magnitude and polarization vary considerably over the 0.25 cm beam height. Averages over the ion trajectory height of the simulations were done for different overall beam center heights and diameters. Good agreement between the averaged simulations and the experimental line shape was obtained for the experimentally expected beam of 0.25 cm diameter centered 0.15 cm above the lower boundary of the rectangular coaxial transmission line.

In the simulations, the SOF evolution operator was approximated by a product of constant field evolution operators. The Bloch-Siegert shift was calculated by substituting the appropriate first-order shift of the counter rotating term in each constant field evolution operator.[25] The resultant shift of the simulated signal was calculated at several symmetric point pairs on the line. This Bloch-Siegert shift calculation was checked by performing a full integration of the Schrödinger equation including the counter-rotating term. The full simulations were averaged over entry phases of every 20° in addition to the average over the trajectory height. The agreement between the first order and full simulation results for the interference signal Bloch-Siegert shifts were better than 5% for the large shifts at the high-power level. The ac Stark shift was calculated by including the appropriate first-order shifts due to couplings with the $4\,^2P_{3/2}$ states in each constant field evolution operator of the simulations. The ac Stark shift and the Bloch-Siegert shift have opposite signs. Table IV gives the calculated total shift (the combined Bloch-Siegert and ac Stark shift). The sources of the quoted uncertainty are the 0.17 mm uncertainty in the beam position, the 5% uncertainty in the absolute power, and the difference between the first order and full Bloch-Siegert calculations. The uncertainty in the beam position is the dominant source of uncertainty for the large, high-power configuration.

Because of time dilation, the frequency in the rest frame of the moving ion is different from the laboratory

TABLE IV. Summary of the corrected interference signal centers. (All entries are in MHz.)

Configuration	Power	Power corrected center[a]	Statistical uncertainty	Power correction uncertainties	ac Stark shift	Detector nonlinearity uncertainties	Beam shift uncertainties	Final corrected center[a]
0 cm	high	70.635	0.026	0.091	1.693(210)	0.025	0.26	68.94(0.35)
0 cm	medium	69.696	0.038	0.145	0.590(70)	0.080	0.44	69.11(0.48)
0 cm	low	70.062	0.110	0.181	0.154(41)	0.090		
0.32 cm	high	70.967	0.030	0.061	1.094(120)	0.015	1.01	69.87(1.02)
0.32 cm	medium	69.977	0.053	0.126	0.386(48)	0.065	0.76	69.59(0.78)
0.64 cm	high	69.093	0.062	0.055	0.767(94)	0.042	0.13	68.33(0.19)

[a]Minus 1700 MHz.

frequency. The correction to be added to the frequency measured in the laboratory frame is given by

$$\tfrac{1}{2}(v/c)^2 f_0 ,$$

where f_0 is the measured frequency. With the measured 121.3(6.3)-keV energy of the beam, the time dilation shift is 0.115(6) MHz. Because this correction is identical for all configurations, it is applied at the end of this section. The 30-mG residual magnetic field of the earth and stray electric fields can shift the Lamb-shift transition frequency. Sources of electric fields are the space charge of the ion beam and the build-up of charge on insulating surfaces. Consideration of these shifts is given in Ref. 25 where they are shown to be less than 5 kHz. This is much less than other uncertainties and can be neglected. A nonlinearity of the photodetector would produce an error in the subtraction of the quenched from the unquenched signal. A test of the photodetector provided an upper bound for the nonlinearity. With this upper bound it is estimated that at most 1% of the normalized quench signal could still be present in $I_{\rm sub}$. The effect of a 1% admixture of $(N_q^{\rm off}/N_{\rm nq}^{\rm off})I_q$ in $I_{\rm sub}$ is calculated for all the narrow separation configurations and listed as an uncertainty in Table IV. Systematic errors in the relative power between the 0° and 180° states could produce a small spurious signal. This spurious signal is known as the incomplete $\bar{Q}$ subtraction (IQS) because it results from an incomplete subtraction of the 0° and 180° quench curves. From the microwave measurements, an estimate of its size can be obtained. The estimate indicated the IQS signal was less than the noise in most of the data and produced a maximum shift in the 0.64 cm configuration of less than 5 kHz. This shift can be neglected. In addition, no IQS contribution was observed at the wide-separation configurations.

To determine the degree with which the subtraction technique was correcting for overlapping transitions in higher n states observed through cascades, data were collected with the two microwave fields separated by 2.29 and 2.92 cm. The simulations indicated that the subtracted $n=4$ Lamb-shift signals should be, respectively, 0.015% and 0.003%. Figure 6 shows the experimental signals for the widely separated oscillatory fields. The measured signal sizes of 0.063% and 0.041%, respectively, are much larger than expected and indicate a failure of the subtraction technique. In addition the subtracted wide-separation signals are not simply a fractional multiple of the quenched or unquenched data. Simulations showed that due to the large matrix elements of the potential $n \geq 5$ cascade transitions, coupling strengths at the high-power level were large enough to produce non-negligible cascade interference signals over 1 GHz away from the cascade transition center frequency. The phase and period of these highly saturated interference signals depended on the microwave power and the distance from the transition center frequency. Because of the complexity of the saturated, high n interference signals, it was not possible to determine on which cascade transition(s) the subtraction technique failed.

In the course of taking data, it was discovered that the line center of the interference signal depended on the magnitude of the beam current. To investigate this effect, several reduced beam current runs at 2 μA (one-third the normal 6 μA beam current) were taken at each experimen-

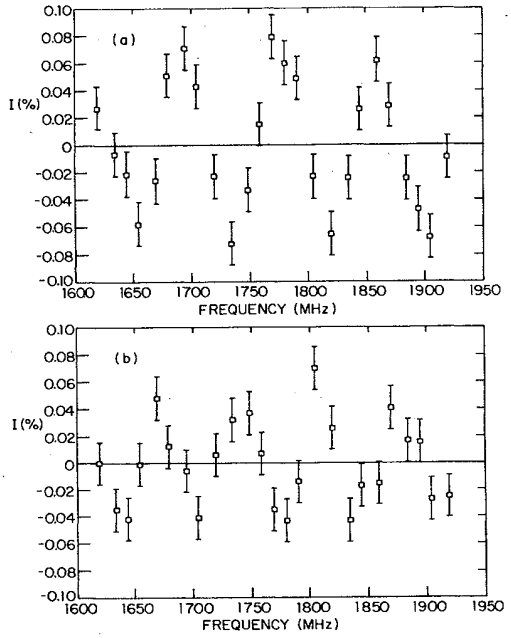

FIG. 6. Wide-separation, high-power, subtracted interference signal at (a) 2.29 and (b) 2.92 cm separation.

tal configuration except the 0.00 cm, low-power configuration. For a given symmetric point pair, the measured shifts (beam shifts) of the symmetric points line center were equal within the statistics of the measurement. In addition, the beam shifts for all the symmetric points pairs in a given experimental configuration were equal to within the statistics of the measurement. The beam shift was simply a shift of the interference signal line center. The size of the beam shift, though, depended strongly on the experimental configuration.

By investigation of the differences between the high and low beam quenched, unquenched, and subtracted interferences signals, the possibility of a Stark shift of the $n=4$ Lamb shift was ruled out. One explanation of the beam shift assumes that some of the overlapping cascade signals are not fully subtracted and enter I_{sub}. For $n \geq 6$, the space charge of a 6 μA beam of 0.25 cm diameter significantly mixes opposite parity states with the same total angular momentum. Lowering the beam current reduces the space charge field and decreases the mixing of these high n states. This will change their cascade contribution to I_{nq}. If the subtraction is not completely working, the high n, cascade contribution to I_{sub} will also be changed. This will give beam shifts which depend on the shape of the cascade signal and therefore depend on the experimental configuration. Given the evidence in the wide-separation data that the subtraction technique is failing, the above hypothesis for the beam shift is reasonable.

In the hypothesis discussed in the previous paragraph, the natural inclination to extrapolate to zero-beam current could give the incorrect answer. If the beam shift is due to a failure of the subtraction technique, a proper analysis of the data would use the high-beam symmetric point centers and calculate the effect of the subtraction failure from the wide-separation data. It is not possible to determine whether the above hypothesis for the beam shift is entirely correct. To account for the incompleteness in the understanding of the beam shift, in each experimental configuration a beam shift uncertainty equal to the difference in the high- and low-beam current centers is assigned to the interference signal line center. Table IV lists the beam shifts as uncertainties in the line center. The corrected centers including the beam shift uncertainties are given in the last column of Table IV.

Because the exact cause of the subtraction failure was not determined, the Lamb-shift transition frequency was determined from the narrow configuration line centers without explicitly correcting each line center for the subtraction failure. The effect of the incompletely subtracted (residual) cascade signal on a narrow separation interference line center depends on the size of the residual signal and its phase at the $n=4$ Lamb-shift transition frequency (1769 MHz). Because the phase of the residual signal at 1769 MHz depends on the separation between the plates, the 0.00, 0.32, and 0.64 cm separation line centers contain different residual signal contributions of possibly opposite sign. The different residual signal contributions will tend to cancel in the average of the line centers, resulting in a smaller contribution of the residual signal to the average line center. It is estimated that the uncertainty produced by the residual signal contribution to the average of the narrow separation high-power line centers is 0.56 MHz.[25] Because no wide-separation data were taken with medium or low power, the uncertainty produced by the residual signal contribution when the medium- and low-power narrow-separation line centers are included in the average could not be estimated. Consequently only the high-power narrow-separation line centers were used to determine the Lamb-shift transition frequency. From Table IV, the average of the high-power narrow-separation line centers is 1769.05(0.63) MHz. When this value is corrected for the 0.115(6) MHz time dilation correction and the 0.56 MHz subtraction failure uncertainty is included, the final value for the $^4\text{He}^+ 4\,^2S_{1/2}$-$4^2P_{1/2}$ Lamb shift is

$$\nu(4\,^2S_{1/2}\text{-}4\,^2P_{1/2}) = 1769.16(0.84)\ \text{MHz}\ .$$

V. CONCLUSIONS

The final value for the Lamb shift is in good agreement with the previous experimental determinations and the theoretical values for this interval (see Table I). This measurement is more precise than the two previous direct experimental determinations of this interval and is comparable in precision to the two indirect measurements. Unfortunately, the precision of the measurement is not good enough to test sensitively the theoretical calculations. Both the Erickson and Mohr value of 1769.13 and 1768.19 MHz lie well within the uncertainty of this experiment.

TABLE V. Summary of the uncertainties in the Lamb-shift measurement. (All frequencies are in MHz.)

Configuration	Line center[a]	Statistical uncertainties	Power correction uncertainties	ac Stark shift uncertainties	Detector nonlinearity uncertainties	Beam shift uncertainties	Subtraction failure uncertainties
0 cm, high	68.94	0.026	0.091	0.210	0.025	0.26	
0.32 cm, high	69.87	0.030	0.061	0.120	0.015	1.01	
0.64 cm, high	68.33	0.063	0.055	0.094	0.042	0.13	
	69.05	0.025	0.071	0.150	0.030	0.607	0.56

[a]With 0.115(6) MHz for time dilation, the final value for the $4\,^2P_{1/2}$-$4\,^2P_{1/2}$ Lamb-shift interval is 1769.16(0.84) MHz.

Table V summarizes the uncertainties of the Lamb-shift measurement. The beam shift and subtraction failure dominates the total uncertainty. An understanding of the beam shift and subtraction failure would reduce the uncertainty of the experiment to 0.17 MHz (100 ppm). By constructing better SOF interaction regions, the ac Stark shift and power correction uncertainty can be reduced by over a factor of 2. This would make possible a 50 ppm determination of the $n=4$ $^4He^+$ Lamb shift.

ACKNOWLEDGMENTS

This research was supported in part by the National Science Foundation through Grant No. PHY78-09657 and PHY80-26547. We would like to thank Randy Knize for his thoughtful assistance with many aspects of this experiment. Special thanks go to Donald Spector for his expert help with the computer simulations and Jaroslaw Olesiak for his careful work on the microwave measurements.

*Present address: Time and Frequency Division, National Bureau of Standards, Boulder, Colorado 80303.

[1]S. R. Lundeen and F. M. Pipkin, Phys. Rev. Lett. **46**, 232 (1981).

[2]G. Newton, D. A. Andrews, and P. J. Unsworth, Philos. Trans. R. Soc. London **290**, 373 (1979).

[3]Yu. L. Sokolov and V. P. Yakovlev, Zh. Eksp. Teor. Fiz. **83**, 15 (1982) [Sov. Phys.—JETP **56**, 7 (1982)].

[4]Yu. L. Sokolov (private communication).

[5]G. W. Erickson, J. Phys. Chem. Ref. Data **6**, 831 (1977).

[6]P. J. Mohr, in *Beam-Foil Spectroscopy,* edited by I. A. Sellin and D. J. Pegg (Plenum, New York, 1976), pp. 89—96.

[7]J. Sapirstein, Phys. Rev. Lett. **47**, 1723 (1981).

[8]G. Carboni, G. Gorini, G. Torelli, L. Palffy, F. Palmonari, and E. Zavattini, Nucl. Phys. A **278**, 381 (1977).

[9]E. Borie and G. A. Rinker, Phys. Rev. A **18**, 324 (1978).

[10]I. Sick, J. S. McCarthy, and R. R. Whitney, Phys. Lett. **64B**, 33 (1976).

[11]E. Lipworth and R. Novick, Phys. Rev. **108**, 1434 (1957) [$S(n=2)=14040.2(1.8)$ MHz].

[12]M. A. Narasimham and R. L. Strombotne, Phys. Rev. A **4**, 14 (1971) [$S(n=2)=14046.2(1.2)$ MHz].

[13]G. W. F. Drake, S. P. Goldman, and A. van Wijngaarden, Phys. Rev. A **20**, 1299 (1979) [$S(n=2)=14040.2(2.9)$ MHz].

[14]D. L. Mader, M. Leventhal, and W. E. Lamb, Jr., Phys. Rev. A **3**, 1832 (1971) [$S(n=3)=4183.17(54)$ MHz].

[15]C. W. Fabjan and F. M. Pipkin, Phys. Rev. A **6**, 556 (1972).

[16]K. A. Safinya, K. K. Chan, S. R. Lundeen, and F. M. Pipkin, Phys. Rev. Lett. **45**, 1934 (1980).

[17]D. A. Van Baak, B. O. Clark, S. R. Lundeen, and F. M. Pipkin, Phys. Rev. A **22**, 591 (1980).

[18]A. Eibofner, Phys. Lett. **58A**, 219 (1976).

[19]R. R. Jacobs, K. R. Lea, and W. E. Lamb, Jr., Phys. Rev. A **3**, 884 (1971).

[20]A. Eibofner, Z. Phys. A **277**, 225 (1976).

[21]G. W. Erickson (private communication).

[22]H.-J. Beyer, in *Progress in Atomic Spectroscopy,* edited by W. Hanle and H. Kleinpoppen, (Plenum, New York, 1978), Pt. A, pp. 529—605.

[23]N. F. Ramsey, *Molecular Beams* (Oxford University, London, 1956).

[24]H. Metcalf and W. Phillips, Opt. Lett. **5**, 540 (1980).

[25]J. J. Bollinger, Ph.D. thesis, Harvard University, 1981.

[26]J. J. Bollinger and F. M. Pipkin, Rev. Sci. Instrum. **52**, 938 (1981).